Mathematical Models of Cell Invasion Track Spatial Position and Progression through the Cell Cycle

By Matthew J. Simpson

Spatial spreading of cell populations is crucial for embryonic development, tissue repair, and malignant invasion. During embryonic development, functional structures—such as various types of tissues and organs—evolve from an initially homogeneous population of cells in the very early embryo. Normal development requires that these structures arise with the correct cell types in the appropriate three-dimensional geometry, a process that necessitates simultaneous migration and growth of cell populations. Abnormal cell migration during adulthood is associated with pathological conditions like cancer invasion and metastasis. While motility of individual cells is crucial for population-level spreading, cell proliferation plays an important—and sometimes overlooked—role in driving spatial expansion of cell populations [4].

Previous researchers have employed both continuum differential-equation models and discrete models that use lattice-based random walks, lattice-free random walks, and cellular automata to mathematically model spatial spreading in cell populations. Continuum mathematical models of combined cell motility and proliferation are often based on the Fisher-Kolmogorov equation [3-4, 6]. We can write this equation in one dimension as

$$\frac{\partial s}{\partial t} = D\frac{\partial^2 s}{\partial x^2} + \lambda s\left(1-\frac{s}{K}\right), \qquad (1)$$

where $s(x,t)>0$ represents cell density, $D>0$ is cell diffusivity, $\lambda>0$ signifies cell proliferation rate, and $K>0$ denotes the environment's carrying capacity density. This simple mathematical model supposes that cells undergo an unbiased random walk and proliferate logistically so that some initial density will evolve—through a combination of diffusion and carrying capacity limited growth—to produce moving fronts. Such fronts lead to the colonization of initially-vacant regions that will eventually reach carrying capacity density K. For certain initial and boundary conditions, (1) can yield travelling wave solutions [4]. This type of modelling framework has successfully described a range of phenomena related to collective cell spreading and cell invasion, from the study of simple *in vitro* scratch assays to *in vivo* malignant brain tumour progression.

In 2008, the introduction of a novel experimental methodology called the Fluorescent Ubiquitination-based Cell Cycle Indicator (FUCCI) [5] enabled real-time analysis of the cell cycle. FUCCI provides spatial and temporal information about the cell cycle's progression through fluorescent probes that glow red when the cell is in the first gap (G1) phase of the cycle and green when in the synthesis (S), second gap (G2), or mitotic/cell division (M) phase [5, 9].

Figure 1a depicts still images from a time-lapse movie of a FUCCI-transduced melanoma cell that illustrate these colour changes during the cell cycle. A visual comparison of the phase contrast image of a C8161 melanoma spheroid (see Figure 1b) and a corresponding FUCCI-transduced spheroid (see Figure 1c) confirms that the FUCCI system reveals a great deal about the relationship between spatial location and the cell cycle. For example, freely cycling cells—indicated by the mixture of red and green fluorescence—are visible on the FUCCI spheroid's outer shell. Upon looking deeper into the spheroid, we observe cells that are largely arrested in the G1 (red) phase, presumably due to a lack of nutrients such as oxygen. The spheroid's centre completely lacks fluorescence; this indicates the presence of a necrotic core. Unsurprisingly, FUCCI technology has revolutionized the analysis of cell proliferation and has applications in experimental models of cancer, stem cell, and developmental biology [9].

We have recently sought to develop and validate continuum models of cell invasion for use with FUCCI technology [7-8]. We employ FUCCI-transduced C8161 melanoma cells and perform a series of scratch assays to observe cell migration; these assays involve creating a "scratch" in a cell monolayer and capturing images close to the scratch at regular intervals. Next we attempt to quantitatively describe these experiments with a new continuum model — a generalisation of the Fisher-Kolmogorov equation.

Figure 2a shows a population of FUCCI-transduced C8161 melanoma cells on a two-dimensional substrate following the creation of a 0.5 millimeter artificial scratch in the population. Figure 2d displays the same experiment after 18 hours; now we see that the cells have moved into the initially-vacant region while continuing to progress through the cell cycle. To model these experiments, we suppose that the cell population—with total density $s(x,t)$—consists of two subpopulations, yielding $s(x,t)=v_r(x,t)+v_g(x,t)$. Here $v_r(x,t)$ is the red cell density in the G1 phase and $v_g(x,t)$ is the green cell density in the S/G2/M phases. Assuming that both subpopulations undergo diffusive migration and proceed through the cell cycle, we encode this information into a generalisation of the Fisher-Kolmogorov equation given by

$$\frac{\partial v_r}{\partial t} = \mathcal{D}_r\frac{\partial^2 v_r}{\partial x^2} - \kappa_r v_r + 2\kappa_g v_g\left(1-\frac{s}{K}\right), \qquad (2)$$

$$\frac{\partial v_g}{\partial t} = \mathcal{D}_g\frac{\partial^2 v_g}{\partial x^2} - \kappa_g v_g\left(1-\frac{s}{K}\right) + \kappa_r v_r, \qquad (3)$$

where $\mathcal{D}_r>0$ is the diffusivity of cells in the G1 phase, $\mathcal{D}_g>0$ is the diffusivity of cells in the S/G2/M phases, $\kappa_r>0$ is the rate of cell transition from the G1 phase to the S/G2/M phases, and $\kappa_g>0$ is the rate of cell transition from the S/G2/M phases to the G1 phase.

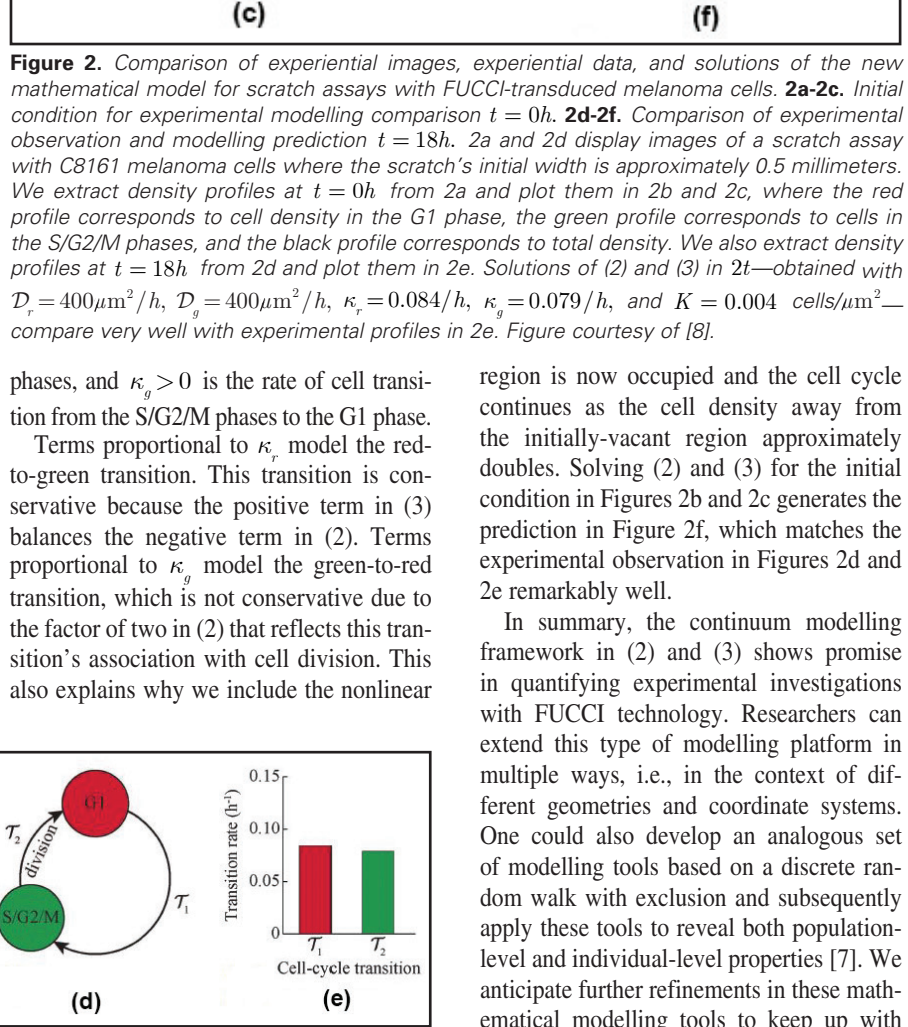

Figure 2. *Comparison of experiential images, experiential data, and solutions of the new mathematical model for scratch assays with FUCCI-transduced melanoma cells.* **2a-2c.** *Initial condition for experimental modelling comparison $t=0h$.* **2d-2f.** *Comparison of experimental observation and modelling prediction $t=18h$. 2a and 2d display images of a scratch assay with C8161 melanoma cells where the scratch's initial width is approximately 0.5 millimeters. We extract density profiles at $t=0h$ from 2a and plot them in 2b and 2c, where the red profile corresponds to cell density in the G1 phase, the green profile corresponds to cells in the S/G2/M phases, and the black profile corresponds to total density. We also extract density profiles at $t=18h$ from 2d and plot them in 2e. Solutions of (2) and (3) in 2t—obtained with $\mathcal{D}_r=400\mu\mathrm{m}^2/h$, $\mathcal{D}_g=400\mu\mathrm{m}^2/h$, $\kappa_r=0.084/h$, $\kappa_g=0.079/h$, and $K=0.004$ cells/$\mu\mathrm{m}^2$—compare very well with experimental profiles in 2e. Figure courtesy of [8].*

Terms proportional to κ_r model the red-to-green transition. This transition is conservative because the positive term in (3) balances the negative term in (2). Terms proportional to κ_g model the green-to-red transition, which is not conservative due to the factor of two in (2) that reflects this transition's association with cell division. This also explains why we include the nonlinear logistic parameter in terms proportional to κ_g, since this event would require sufficient space to accommodate the daughter agent. Our result is directly analogous to the per capita proliferation rate in the Fisher-Kolmogorov equation existing as a linearly decreasing function of total density.

To determine whether (2) and (3) can predict the spatial and temporal dynamics of the scratch assay in Figure 2a, we divide each image of the assay into a series of equally-spaced columns. Counting the number of red and green cells per column and dividing by the area of the column estimates the total cell density (see Figure 2b) and the density for both the red and green subpopulations. The density profile in 2e portrays the system's state after 18 hours. Two main outcomes are apparent: the initially-vacant region is now occupied and the cell cycle continues as the cell density away from the initially-vacant region approximately doubles. Solving (2) and (3) for the initial condition in Figures 2b and 2c generates the prediction in Figure 2f, which matches the experimental observation in Figures 2d and 2e remarkably well.

In summary, the continuum modelling framework in (2) and (3) shows promise in quantifying experimental investigations with FUCCI technology. Researchers can extend this type of modelling platform in multiple ways, i.e., in the context of different geometries and coordinate systems. One could also develop an analogous set of modelling tools based on a discrete random walk with exclusion and subsequently apply these tools to reveal both population-level and individual-level properties [7]. We anticipate further refinements in these mathematical modelling tools to keep up with new advances in experimental cell biology.

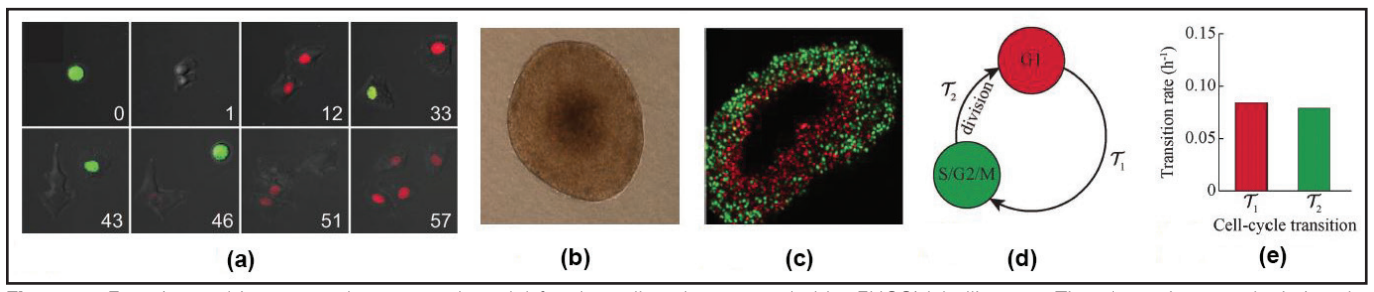

Figure 1. *Experimental images and conceptual model for the cell cycle as revealed by FUCCI labelling.* **1a.** *Time lapse images depicting the progression of three generations of FUCCI-transduced C8161 melanoma cells through the cell cycle. The numbers in each subfigure indicate the time in hours.* **1b.** *Phase contrast image of a C8161 melanoma spheroid with an approximate diameter of 0.5 millimeters.* **1c.** *Image of a slice of a C8161 melanoma spheroid of, similar size to 1b where the cells are transduced with FUCCI.* **1d.** *Conceptual model of FUCCI technology.* **1e.** *Experimental data presenting quantification of the rate of red-to-green and green-to-red transitions for the C8161 melanoma cell line. 1a courtesy of [2], 1b and 1c courtesy of [1], 1d and 1e courtesy of [8].*

References

[1] Beaumont, K.A., Anfosso, A., Ahmed, F., Weninger, W., & Haass, N.K. (2015). Imaging- and flow cytometry-based analysis of cell position and the cell cycle in 3D melanoma spheroids. *J Vis. Exp., 106*, e53486.

[2] Haass, N.K, Beaumont, K.A., Hill, D.S., Anfosso, A., Mrass, P., Munoz M.A.,…Weninger, W. (2014). Real-time cell cycle imaging during melanoma growth, invasion, and drug response. *Pig. Cell Melan. Res., 27*, 764-776.

[3] Jin W., Shah, E.T., Penington, C.J., McCue, S.W., Chopin, L.K., & Simpson, M.J. (2016). Reproducibility of scratch assays is affected by the initial degree of confluence: experiments, modelling and model selection. *J. Theor. Biol., 390*, 136-145.

[4] Maini, P.K., McElwain, D.L.S., & Leavesley, D.I. (2004) Traveling wave model to interpret a wound-healing cell migration assay for human peritoneal mesothelial cells. *Tissue Eng., 10*, 475-482.

[5] Sakaue-Sawano, A., Kurokawa, H., Morimura T., Hanyu, A., Hama, H, Osawa, H,…Miyawaki, A. (2008). Visualizing spatiotemporal dynamics of multicellular cell-cycle progression. *Cell, 132*, 487-498.

[6] Sherratt, J.A, & Murray, J.D. (1990). Models of epidermal wound healing. *Proc. R. Soc. Lond. B., 249*, 29-36.

[7] Simpson, M.J., Jin, W., Vittadello, S.T, Tambyah, T.A., Ryan, J.M., Gunasingh, G., …McCue, S.W. (2018). Stochastic models of cell invasion with fluorescent cell cycle indicators. *Physica A., 510*, 375-386.

[8] Vittadello, S.T., McCue, S.W., Gunasingh, G., Haass, N.K, & Simpson, M.J. (2018). Mathematical models for cell migration with real-time cell cycle dynamics. *Biophys J., 114*, 1241-1253.

[9] Zielke, N., & Edgar, B.A. (2015). FUCCI sensors: powerful new tools for analysis of cell proliferation. *WIREs Dev Biol., 4*, 469487.

Mat Simpson is a professor of applied mathematics at Queensland University of Technology in Australia. His research interest is broadly in the area of mathematical biology, with specific attention to stochastic modelling, computational mathematics, and experimental cell biology.